Article

Spall behavior of steels under hypervelocity impact

Tatsumi MORITOH*, Shohei MATSUOKA*, Toshiyuki OGURA*,
Kazutaka G. NAKAMURA*, Ken-ichi KONDO*, Masahide KATAYAMA**,
and Masatake YOSHIDA***

We performed hypervelocity impact experiments on steel materials (SS400, SUS304, and SCM440) at velocities up to 9 km s^{-1}. Microstructure and micro damages near a crater and on the spall plane were examined using optical microscopy and scanning electron microscopy. The α-ε phase transition region was observed near the crater of SS400 and SCM440 samples recovered. Cracks which are parallel to the impact direction below the crater were observed, and radial cracks grew from the α-ε phase interface at high velocity impact tests. Cleavage was dominant mechanism for a spall fracture surface of both of SS400 and SCM440, while ductile fracture was observed at the fracture surface of SUS304. Geometric spall behaviors were compared with numerical simulations using hydrocode. Spall diameters were well reproduced by optimizing yield strength for each steel at high impact velocities, particularly above 6 km s^{-1}. Spall strength was determined to be 1.1, 2.7, and 2.1 GPa for SS400, SUS304, and SCM440, respectively.

1. Introduction

Dynamic loadings such as detonation of high explosive and hypervelocity impact induce spall fractures near the rear surface of the target. The spall is defined as rupture within a body due to stress states in excess of the tensile strength of the material[1]. Several parameters such as strain rate[2] and initial temperature[3] have been found to change the spall behavior. The spall behaviors of many kinds of steel have been studied for its industrial uses and developments of a bumper system to assess the protection of orbital space debris impacts on the spacecraft. Steel materials are also of interest in connection with martensitic transformation[4], formation of adiabatic shear band[5], and ductile-brittle transition[6] under dynamic high-pressure loading. Dynamic phase transition from the α-phase (bcc) to the ε-phase (hcp) in pure iron and ferritic steels has been reported to occur at around 13 GPa[7].

Although gas guns are of advantage to impact experiments compared with flyer acceleration using laser shock technology because of its ability to accelerate a heavy projectile weighing more than several hundreds of milligram without changing initial state of the flyer materials such as initial temperature, almost conventional two-stage light-gas guns are limited to launch at velocities less than 7 km s^{-1}. We developed a compact two-stage light-gas gun, which could accelerate a projectile weighing 0.6 gram up to 8.9 km s^{-1} using hydrogen as a driver gas, having the total length of 12 m[8].

In this work, we performed hypervelocity impact experiments of three steels at the room temperature in the velocity range of 3-9 km s^{-1} by

Received : May 17, 2002
Accepted : December 11, 2002
*Materials and Structures Laboratory, Tokyo Institute of Technology
4259 Nagatsuta, Midori, Yokohama, 226-8503, Japan
telephone and fax +81(45)924-5382,
e-mail moritoh@kkhp8.rlem.titech.ac.jp
**CRC Solutions Corp.
2-7-5 Minamisuna, Koto-ku, Tokyo, 136-8581, Japan
telephone +81(3)5634-5774, fax +81(3)5634-7340,
e-mail autodyn@crc.co.jp
***National Institute of Advanced Industrial and Science Technology (AIST)
1-1 Higashi, Tsukuba, Ibaraki 305-8565, Japan
telephone +81(298)61-4792, fax +81(298)61-4783,
e-mail m-yoshida@aist.go.jp

using this gun. The purpose of this study is to examine the differences in spall behavior of three kinds of steel experienced dynamic loadings. Numerical simulations using hydrocode were also performed to investigate fracture mechanism.

2. Experimental and Numerical Simulation

Impact experiments ware made by using the two-stage light-gas gun[8]. The impact velocity was measured by Magnetoflyer method[9]. Polycarbonate was used as the projectile material, and a small magnet was embedded in the sabot for projectile velocity measurement. The sabot is 11.85-mm in diameter, and its mass varied from 0.6 g to 1.7 g by varying its length from 4 mm to 12 mm, respectively. The samples used were SS400, SUS304, and SCM440: SS400 steel is a ferritic steel, which has a microstructure consisting of a dispersion of cementite particles embedded in ferrite particles, SUS304 is an austenitic steel which has fcc structure, and SCM440 is a steel quenched at 850 K. Chemical composition and mechanical properties of these steels are listed in Table 1. The target size was 70 mm in diameter, and 20 mm or 30 mm in thickness. After impact, the targets ware recovered, spark cut just across the crater center, polished, and sometimes etched by 10-cm^3 conc. nitric acid in 90-cm^3 ethanol solution. Microstructure and micro damages were examined using optical microscopy and scanning electron microscopy, and the spall diameter was measured.

A two-dimensional hydrocode, AUTODYN-2D (Century Dynamics Inc.), was used to simulate impact phenomena. The Eulerian frame of reference was applied to compare the geometric spall behaviors and internal failures with the experimental results. Mie-Gruneisen form of the shock Hugoniot equation of state was applied for all materials. Material strength models for projectile were assumed to be hydrodynamic, and the Steinberg-Guinan model was applied for steels. Because material properties of Steinberg-Guinan model for SS400 and SCM440 are not reported, those of SUS304 and SS21-6-9 steel were used, respectively. Initial densities for each steel were defined by those listed in Table 1. We used a failure model, in which the material failure occurs by a hydrostatic tensile stress, as a spall fracture criteria. The spall strength was determined by changing yield stress in order to reproduce a spall diameter at the maximum impact velocity for each steel.

3. Experimental Results and Discussions

Polished and etched cross sections of 30-mm thick SS400 target impacted at different velocities are shown in Fig. 1. The depth and diameter of crater were dependent on strongly impact velocity and sabot thickness, respectively. At the rear surface, spall fracture, which the diameter increased with increasing impact velocity, was observed. A crater depth, a crater diameter, a maximum spall depth, and a spall diameter of SS400 impacted at 8.8 km s^{-1} with a 4-mm thick sabot were 11.0, 25.8, 4.9, and 50.0 mm, respectively. There were cracks parallel to the impact direction of the projectile as well as those extending from the crater surface into the target below the crater. It is also found that there were radial cracks especially in targets impacted at high velocity above 6 km s^{-1}. All of the impacted targets etched showed a crescent-shaped white region

Table 1 Chemical composition and mechanical properties of steels used

Chemical composition (wt%)			
SS400	Fe -0.1 C-0.05>P-0.05>S		
SUS304	Fe-0.08>C-1.0>Si-2.0>Mn-9 Ni-19 Cr		
SCM440	Fe-0.4 C-0.7 Mn-1.0 Cr-0.25 Mo		
Mechanical properties			
	SS400	SUS304	SCM440
Density (g·cm^{-3})	7.9	8.0	7.8
Young modulus (GPa)	206	197	–
Yield strength (MPa)	240	205	833
Tensile strength (MPa)	450	520	980

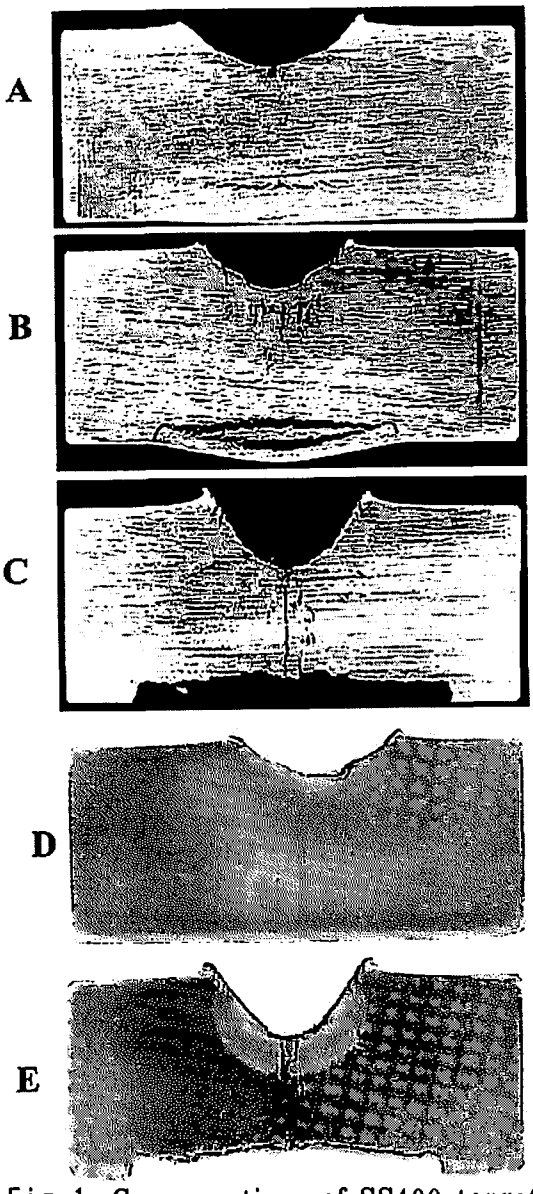

Fig. 1 Cross sections of SS400 target impacted at different velocities. (A) Polished, sabot length was 12 mm; impact velocity was 4.1 km s^{-1}. (B) Polished, sabot length was 5 mm; impact velocity was 5.9 km s^{-1}. (C) Polished, sabot length was 4 mm, impact velocity was 8.8 km s^{-1}. (D) Polished and etched, sabot length was 12 mm, impact velocity was 3.4 km s^{-1}. (E) Polished and etched, sabot length was 4 mm, impact velocity was 8.5 km s^{-1}.

below the crater[5]. The region increased with increasing the impact velocity. Figure 2 shows polished and etched cross sections of three steels. The thickness of sabot and sample used were all 4 mm and 12 mm, respectively. It is found that crater of each steel impacted at an almost same velocity have no big difference, but that there are difference clearly in spall behaviors. In particular, spall fracture of SUS304 is different drastically from those of other two steels, and perfect fracture occurs only at the center region. The crescent-shaped region, which size was almost same to that of SS400 steel impacted at a same velocity, below the crater was observed also at the cross sections of SCM440, while that was not observed in the SUS304 etched in various solutions. These results are consistent with report by Shockey, Curran, and De Carli[5]. There were also radial cracks at the cross sections of SCM440. It is suggested that these radial cracks are due to the formation of crescent-shaped region.

Figure 3 shows SEM images of the spall fracture plane for each steel. These experiments were performed by using 4-mm thick sabot and 20-mm thick sample. For SS400 steel, cleavage fracture was dominant at the center region of spall plane and a void was not observed, while ductile fracture occurred at the edge of spall plane in the range of sub millimeter. It is suggested that the spall occur mainly by cleavage of ferrite grains, and then the spall region, which was accelerated and moves at several hundred m s^{-1}, would stretch neighboring non-spall region. SUS304 steel shows ductile fracture throughout the spall plane, and many voids with diameter of 5-50 μm were observed. In the case of SCM440, brittle fracture was dominant for the spall plane, and voids with diameter of about 10μm were also observed.

Relationship between the calculated spall diameter and the impact velocity for SS400 steel is shown in Fig. 4 with experimental results. The thickness of sample was 30 mm, and calculations were performed as to both of 4-mm and 12-mm thick sabot. The yield strength of normal SS400 steel is reported to be about 240 MPa. Using this value for yield strength and a spall strength of 1.5 GPa, a spall diameter could be reproduced only at high impact velocity above 6 km s^{-1}. Using the yield stress of 503 MPa and spall strength of 1.1 GPa, the error in the low velocity range became smaller than that obtained by using a value of 240 MPa in both case of 4-mm and 12 mm sabot. It is

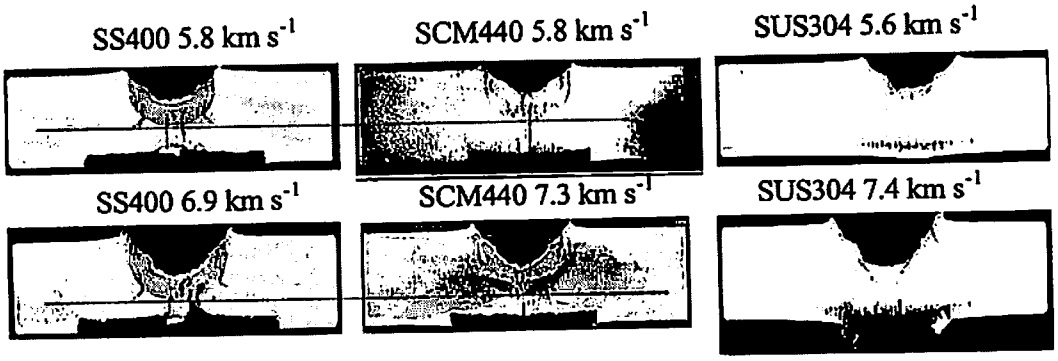

Fig. 2 Polished and etched cross sections of three steels. Kinds of steel and impact velocity are showed above each photograph. Lines are drew in order to compare the sizes of crescent- shaped region observed at both of SS400 and SCM440.

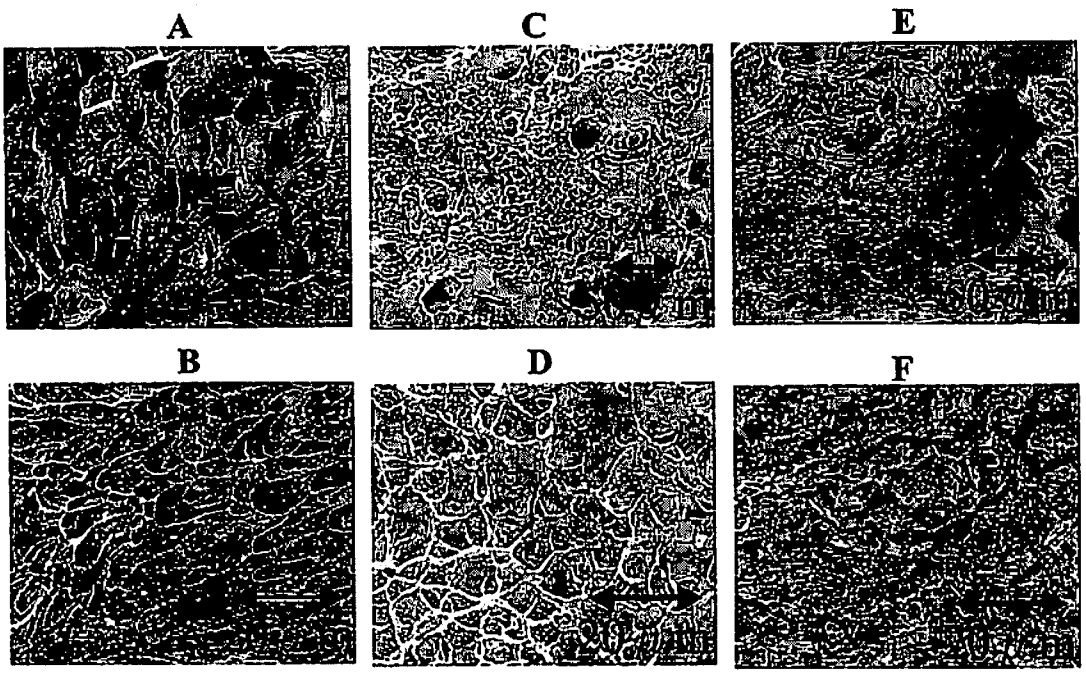

Fig. 3 SEM images of spall fracture plane of each steel. (A) SS400, at the center of spall plane. (B) SS400, at the edge of spall plane. (C) and (D) SUS304. (E) and (F) SCM440.

necessary to optimize yield strength for each material in the calculation using Steinberg-Guinan model. We also calculated bulk failure regions of SS400 steel at 50 μs after impact. It was clear that there are many balk failure regions below crater, which seem to be cracks of the target recovered, in the case of 1.1 GPa, but a few bulk failures occur below the crater in calculations using a spall strength of 2.0 GPa. It is predicted that the cracks below the crater would be due to dynamic tensile stress in the subcrater region. Pressure and temperature profile calculations at the crescent-shaped region observed on etched cross section of SS400 and SCM440 recovered showed that the region reached ε phase under impact. It is expected that the region would experience α-ε phase transition under dynamic loading[5].

Figure 5 shows relationship between the calculated spall diameter and the impact velocity for each steel with experimental results. These experiments were all performed by using 4-mm thick sabot and 20-mm thick sample. The spall diameter of SUS304 steel was defined as a region, which has voids or cracks near the rear surface. It is found that there is big difference in spall behaviors of each steel. The spall strength for

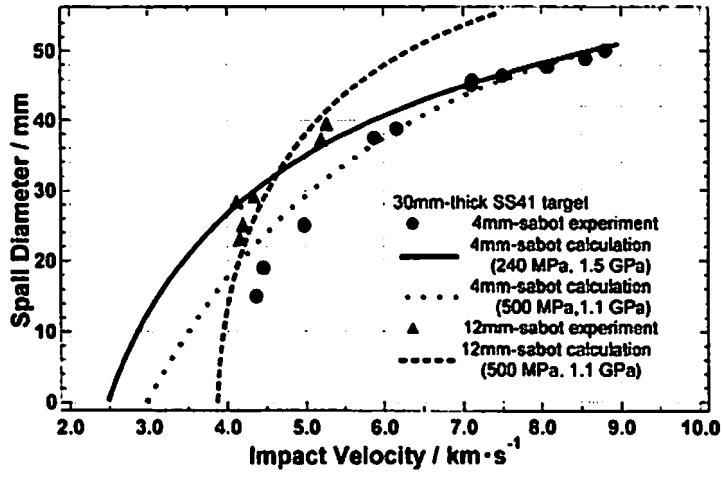

Fig. 4 Effects of yield stress on spall diameter and spall strength of SS400 steel. The solid line was obtained using a yield stress of 240 MPa and a spall strength of 1.5 GPa, while dashed line was obtained using a yield stress of 503 MPa and a spall strength of 1.1 GPa.

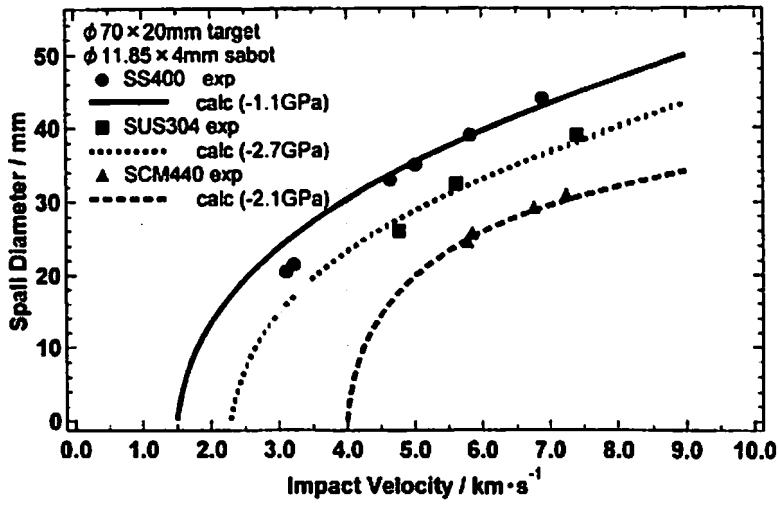

Fig. 5 Relations between spall diameter and impact velocity for each steel. Spall strength was defined to be 1.1 GPa, 2.7 GPa and 2.1 GPa for SS400, SUS304 and SCM440, respectively.

SUS304 and SCM440 was defined to be 2.7 GPa and 2.1 GPa by using a value of 410 MPa and 830 MPa for yield strength, respectively. The obtained value of spall strength for SUS304 is smaller than 3.0 GPa reported by D. J. Steinberg[10]. The spall diameter of each steel at a same impact velocity was not proportional to spall strength, and SUS304 steel have a higher spall strength than that of SCM440, but an impact velocity, which the spall starts to occur, was lower that that of SCM440. This would be due to difference in fracture mechanism.

4. Conclusion

Spall behaviors of SS400, SUS304, and SCM440 at high impact velocities particularly above 6 km s-1 are well reproduced by using hydrocode calculation. It is necessary to optimize other material parameters in order to reproduce spall diameters at low impact velocities. The spall strengths defined by using AUTODYN-2D for each steel were not proportional to each normal yield

strength. Perfect spall fracture occurs at all over the area, in which materials reach to stress level necessary for brittle fracture, in the case of SS400 and SCM440. The spall strength of SUS304 steel, in which the ductile fracture is dominant, will be related to a stress level necessary for nucleation of voids, and growth and coalescence stages (perfect spall fracture) will need much more tensile stress or fracture energy. It will be necessary to use different fracture models for each steel, which spall fracture formation occurs by different mechanisms, in calculations using AUTODYN-2D.

Acknowledgments

The authors thank M. Hasegawa for his experimental help.

References

1) D. E. Grady, J. Mech. Phys. Solids. 36, 353(1988).
2) W-S. Lee and C-F. Lin, Mater. Sci. Eng. A 308, 124(2001).
3) K. Baumung, H. Bluhm, G. I. Kanel, G. Muller, S. V. Razorenov, J. Singer, and A. V. Utkin, Int. J. Impact Engng. 19, 189(1997).
4) N. N. Thadhani and M. A. Meyers, Acta. Metall. 34, 1625(1986).
5) D. A. Shockey, D. R. Curran, and P. S. De Carli, J. Appl. Phys. 46, 3766(1975).
6) I. Gilath, S. Eliezer, M. P. Dariel, and Kornblit, Appl. Phys. Lett. 52, 1207(1988).
7) D. Bancroft, E. L. Peterson, and S. Minshall, J. Appl. Phys. 27, 291(1956).
8) T. Moritoh, N. Kawai, K. G. Nakamura, and K. Kondo, Rev. Sci. Instrum. 72, 4270(2001).
9) K. Kondo, A. Sawaoka, and S. Saito, Rev. Sci. Instrum.48, 1581(1977).
10) D. J. Steinberg, "Equation of state And Strength Properties of Selected Materials", UCRL-CMA-C106439, LLNL, (1991).